Globally accurate *ab initio* based potential energy surface of $H_2O^+(X^4A'')$*

Song Yu-Zhi(宋玉志)†, Zhang Yuan(张 媛), Zhang Lu-Lu(张路路), Gao Shou-Bao(高守宝), and Meng Qing-Tian(孟庆田)

College of Physics and Electronics, Shandong Normal University, Jinan 250014, *China*

(Received 4 January 2015; revised manuscript received 28 January 2015; published online 10 April 2015)

A globally accurate potential energy surface is reported for the electronic ground-state H_2O^+. The *ab initio* energies utilized to map the potential energy surface are calculated at the multireference configuration interaction method employing the aug-cc-pVQZ basis set and the full valence complete active space wave function as reference. In order to improve accuracy of the resulting raw *ab initio* energies, they are then extrapolated to the complete basis set limit and most importantly to the full configuration-interaction limit by semiempirically correcting the dynamical correlation using the double many-body expansion-scaled external correlation method. The topographical features of the current potential energy surface were examined in detail, which agree nicely with those of other theoretical work.

Keywords: H_2O^+, multi-reference configuration interaction method, potential energy surface, vibrational frequencies, spectroscopic constants

PACS: 31.15.A–, 31.15.ae, 31.50.Bc **DOI:** 10.1088/1674-1056/24/6/063101

1. Introduction

Due to their importance in planetary ionospheres and interstellar chemistry, ion–molecule reactions have been the subject of a vast amount of studies.[1,2] From the experimental point of view, since it is quite simple to accelerate ions, molecular beam experiments can be carried out relatively easier on such a kind of reaction over a wide range of relative translational energies. However, it is usually difficult to explore the reaction dynamics studies theoretically on such a kind of reaction system, since the energies of ground and excited potential energy surfaces (PESs) are frequently degenerate or close, and the electronically nonadiabatic processes easily occur.[3–5] Among a series of ion–molecule reactions, the $O^+(^4S) + H_2(X\,^1\Sigma_g^+) \rightarrow OH(X\,^3\Sigma^-) + H(^2S)$ reaction is an exceptional case, which mainly takes place adiabatically on the lowest energy quadruplet ($1^4A''$ in C_s symmetry) PES over a quite wide range of collision energy.[3] Thus, the $O^+(^4S) + H_2(X\,^1\Sigma_g^+)$ reaction which is regarded as a prototype of moderately exothermic ion–molecule reactions involving an H atom transfer, has received plenty of studies both experimentally and theoretically.

Experimentally, the rate constants for reactions in which a series of positive ions (O^+, N^+, Ar^+, N_2^+, CO^+, CO_2^+, and N_2O^+) abstract a hydrogen atom from H_2 were measured by Fehsenfeld *et al.*[6] at 300 K in a pulsed, flowing-after glow reaction tube. By using the ion cyclotron resonance and selected ion flow tube techniques separately, the rate constants for the reaction $O^+ + H_2 \rightarrow OH^+ + H$ were obtained by Kim and Smith *et al.*,[7] respectively. Both the rate constants and branching fractions were reported by Viggiano *et al.*[8] for the reaction of O^+ with HD as a function of average center-of-mass kinetic energy at three temperatures: 93, 300, and 509 K. For the state-selected reactions of $O^+(^4S,^2D,^2P) + H_2/D_2$, the absolute total cross sections were measured over the collision energy range of 0.02 eV–12 eV.[9] The total cross sections of $O^+(^4S,^2D,^2P) + HD$ reaction were measured by Sunderlin and Armentrout.[10] The velocity vector distributions for the reactive and nonreactive scattering of O^+ by H_2, HD, and D_2 were reported by Gillen,[11,12] which showed that such a reaction and its isotopic variations proceed from ground-state reactants to predominantly electronic ground state products via a direct interaction. An interesting conclusion can be drawn from the above experimental studies, which is that the electronically nonadiabatic processes, such as charge transfer and dissociative charge transfer, are important only at high collision energies.

Amongst the vast quantity of theoretical work, employing the quasiclassical trajectory (QCT) approach, González *et al.*[13,14] investigated the ion–molecule reaction of $O^+(^4S)$ with $H_2(X\,^1\Sigma_g^+)$ and its isotopic variants (D_2 and HD), based on an empirical surface derived from experimental and *ab initio* information. Using the diatomics-in-molecules (DIM) model, Whitton *et al.*[15] constructed the PES of $H_2O^+(X\,^4A'')$. A more accurate global PES of $H_2O^+(X\,^4A'')$

*Project supported by the National Natural Science Foundation of China (Grant Nos. 11304185 and 11074151), China Postdoctoral Science Foundation (Grant No. 2014M561957), the Postdoctoral Innovation Project of Shandong Province, China (Grant No. 201402013), and the Shandong Provincial Natural Science Foundation, China (Grant No. ZR2014AM022).

†Corresponding author. E-mail: yzsong@sdnu.edu.cn

© 2015 Chinese Physical Society and IOP Publishing Ltd

was established by Martínez *et al.*[4] using many-body expansion (MBE). The properties of the most relevant stationary points of this reaction were analyzed in detail. Subsequently, in order to investigate the dynamics of the $O^+ + H_2$ reaction and its isotopic variants D_2 and HD, they performed the dynamics studies using methods of QCT,[16] time-dependent real wave packet quantum dynamics[17] and time-independent close-coupling hyperspherical (CCH) quantum dynamics[18] based on such PES. Moreover, a lot of other dynamics studies were also performed using this global PES. By using centrifugal sudden (CS) approximation, time-dependent wave packet calculations have been performed by Kłos *et al.*[19] for the $O^+ + H_2$, and exact total reflection probabilities at the total angular momentum $J = 0$ and approximate ones for $J > 0$ have been calculated. Zhang *et al.*[20] studied the influence of coriolis coupling (CC) on the $O^+ + H_2$, showing CC plays an important role in this reaction. The dynamics of the exchange reaction H + OH^+ were also investigated by Zhang *et al.*[21] using the time-dependent wave packet quantum method under CS approximation. The results of dynamics obtained by theoretical calculations can be compared well with the experimental ones.

However, the PES constructed by Martínez *et al.*[4] was obtained by fitting around 600 *ab initio* points calculated at CCSD(T) level with cc-pVQZ basis set. We are also aware that the dissociation energy of $OH^+(X\,^3\Sigma^-)$ was calculated from such PES to be 5.1268 eV, while the experimental value is 5.301 eV, showing a relatively larger difference of 0.1742 eV (~ 4.0172 kcal·mol^{-1}). Compared with the most recent result (5.2816 eV) obtained by Paniagua,[5] the difference is calculated to be 0.1544 eV (~ 3.5606 kcal·mol^{-1}). Thus, we are motivated to constructing more accurate global analytical PES of $H_2O^+(X\,^4A'')$ by fitting more accurate *ab initio* energies to be calculated with multireference configuration interaction (MRCI)[22] level and larger basis set aug-cc-pVQZ[23,24] (denoted as AVQZ). In this work, a realistic global analytical PES for H_2O^+ ($1\,^4A''$) is reported, which is obtained by fitting 2690 *ab initio* points that were calculated at MRCI[22] level of theory, using the full valence complete active space (FVCAS)[25] reference wave function and the Dunning's basis set AVQZ. The resulting *ab initio* energies have been subsequently corrected, using the double many-body expansion-scaled external correlation (DMBE-SEC)[26] method to extrapolate to the one-electron complete basis set (CBS) limit.[27] The PES so obtained shows the correct behavior at all dissociation channels while providing a realistic representation of the surface features at all interatomic separations.

This paper is organized as follows. Section 2 presents the *ab initio* calculations employed in the present work. Section 3 describes the analytical representation of the H_2O^+ ($X\,^4A''$) PES. Main topographical features of the current PES are discussed in Section 4. Finally, Section 5 summarizes the concluding remarks.

2. *Ab initio* calculations

In order to map the H_2O^+ ($X\,^4A''$) PES, a grid of raw 2690 *ab initio* energies has been calculated, which is defined by $1.2 \le R_{H_2}/a_0 \le 3.8$, $1.0 \le r_{O^+-H_2}/a_0 \le 15.0$, and $0.0 \le \gamma/\text{deg} \le 90$ for $O^+ - H_2$ channel; while $1.5 \le R_{OH^+}/a_0 \le 4.0$, $2.0 \le r_{H-OH^+}/a_0 \le 15.0$, and $0.0 \le \gamma/\text{deg} \le 180$ for $H - OH^+$ channel. As described in Ref. [28]–[30], R, r, and γ are the atom–diatom Jacobi coordinates. By using the FVCAS[25] as reference, all *ab initio* calculations have been carried out at the MRCI[22] level. The AVQZ basis set of Dunning has been employed, with the calculations being performed using the Molpro[31] package. C_s point group symmetry is employed in the *ab initio* calculation, which holds two irreducible representations, namely, A′ and A″. For $H_2O^+(X\,^4A'')$, five A′ and one A″ symmetry molecular orbitals (MOs) are determined as the active space, amounting to a total of 172 (110A′ + 62A″) configuration state functions. The molecular orbitals, which correlate with 2s, 2p atomic orbitals of the O^+ ion and the 1s orbital of each H atom, are utilized to determine the valence space. Such a procedure provides a good description of bond formation/breaking which takes place in the reactive process, in which case the CCSD(T) usually fails.

Aiming at accounting for the excitations beyond singles and doubles and, most importantly, for the incompleteness of the basis set, the resulting *ab initio* energies have subsequently been modeled by scaling the external correlation employing the DMBE-SEC method developed by Varandas.[26] According to the DMBE-SEC scheme, the total energy can be written as the following form

$$V(\boldsymbol{R}) = V_{\text{FVCAS}}(\boldsymbol{R}) + V_{\text{SEC}}(\boldsymbol{R}), \tag{1}$$

where

$$V_{\text{FVCAS}}(\boldsymbol{R}) = \sum_i V^{(2)}_{i,\text{FVCAS}}(R_i) + V^{(3)}_{\text{FVCAS}}(\boldsymbol{R}), \tag{2}$$

$$V_{\text{SEC}}(\boldsymbol{R}) = \sum_i V^{(2)}_{i,\text{SEC}}(R_i) + V^{(3)}_{\text{SEC}}(\boldsymbol{R}), \tag{3}$$

where the first terms of Eqs. (2) and (3) sum over all the diatomic components with $i = \text{AB}, \text{BC}, \text{AC}$, and $\boldsymbol{R} = \{R_{\text{AB}}, R_{\text{AC}}, R_{\text{BC}}\}$ in $V^{(3)}_{\text{FVCAS}}(\boldsymbol{R})$ and $V^{(3)}_{\text{SEC}}(\boldsymbol{R})$ is a collective variable of all internuclear distances. $V^{(2)}_{i,\text{SEC}}(R_i)$ and $V^{(3)}_{\text{SEC}}(\boldsymbol{R})$ in Eq. (3) are then expressed as

$$V^{(2)}_{i,\text{SEC}}(R_i) = \frac{V^{(2)}_{i,\text{MRCI}}(R_i) - V^{(2)}_{i,\text{FVCAS}}(R_i)}{F^{(2)}_i}, \tag{4}$$

$$V^{(3)}_{\text{SEC}}(\boldsymbol{R}) = \frac{V^{(3)}_{\text{MRCI}}(\boldsymbol{R}) - V^{(3)}_{\text{FVCAS}}(\boldsymbol{R})}{F^{(3)}}. \tag{5}$$

As is done in the previous work,[32–34] the scaling factors $F_i^{(2)}$ of diatoms in Eq. (4) are chosen to reproduce the corresponding bond dissociation energies of the i-th diatom, while the scaling factor $F^{(3)}$ in Eq. (5) is fixed at the average of three two-body scaling factors. For the AVQZ basis set, such a procedure leads to the two-body and three-body scaling factors as: $F_{H_2}^{(2)} = 0.9845$, $F_{OH^+}^{(2)} = 0.7981$, and $F^{(3)} = 0.8602$.

3. Analytical potential energy function of H_2O^+ ($X\,^4A''$)

Employing the many-body expansion method proposed by Murrell and Carter,[35] the analytical functional form of $H_2O^+(X\,^4A'')$ PES can be expressed as

$$V(R_1,R_2,R_3) = \sum_{i=1}^{3} V_i^{(1)} + \sum_{i=1}^{3} V^{(2)}(R_i) + V^{(3)}(R_1,R_2,R_3), \quad (6)$$

where $V_i^{(1)}$ is the energy for isolated atom, $V^{(2)}(R_i)$ represents the two-body term, and $V^{(3)}$ is the three-body term which becomes zero at all dissociation limits. In the present case, the $H_2O^+(X\,^4A'')$ PES follows the dissociation scheme as

$$H_2O^+(X\,^4A'') \rightarrow \begin{cases} H_2(X\,^1\Sigma_g^+) + O^+(^4X), \\ OH^+(X\,^3\Sigma^-) + H(^2X), \\ 2H(^2S) + O^+(^4X). \end{cases} \quad (7)$$

Thus, the one-body term $V_i^{(1)}$ equals zero since all possible dissociation channels of $H_2O^+(X\,^4A'')$ correlate with the atoms in their ground states (i.e., $H(^2S)$ and $O^+(^4S)$). The two-body terms involve the $H_2(X\,^1\Sigma_g^+)$ and $OH^+(X\,^3\Sigma^-)$, with their analytical expression being represented by the formalism developed by Aguado and Paniagua,[36,37] which was recently applied to construct the $X\,^2\Sigma^+$ and $A\,^2\Pi$ states of CN,[38] can be written as the sum of the short- and long-range potentials,

$$V_{AB}^{(2)} = V_{short}^{(2)} + V_{long}^{(2)}, \quad (8)$$

where

$$V_{short}^{(2)} = \frac{a_0}{R_{AB}} e^{-\beta_1^{(2)} R_{AB}}, \quad (9)$$

which warrants the diatomic potentials tend to infinite value when $R_{AB} \rightarrow 0$. The long-range potential which tends to zero as $R_{AB} \rightarrow \infty$ takes the following expression

$$V_{long}^{(2)} = \sum_{i=1}^{n} a_i \left(R_{AB} e^{-\beta_2^{(2)} R_{AB}} \right)^i. \quad (10)$$

The linear parameters a_i $(i = 1,2,\ldots,n)$ and the nonlinear parameters β_i $(i = 1,2)$ in Eqs. (9) and (10) are obtained by fitting the *ab initio* potential energies of the diatoms. All the coefficients used to model the diatomic potentials for $OH^+(X\,^3\Sigma^-)$ and $H_2(X\,^1\Sigma_g^+)$ are gathered in Table 1. While, the properties of both the OH^+ and H_2 potential energy curves (PECs), including equilibrium geometries, dissociation energies, vibrational frequencies, and spectroscopic constants are gathered in Table 2, which agree excellently with other theoretical and experimental values. Shown in Fig. 1 are the $OH^+(X\,^3\Sigma^-)$ and $H_2(X\,^1\Sigma_g^+)$ PECs, which mimic the *ab initio* potential energies nicely, showing accurate and smooth behavior both in short and long regions.

Table 1. Fitted parameters of two-body energy term in Eq. (10).

	$OH^+(X\,^3\Sigma^-)$	$H_2(X\,^1\Sigma_g^+)$
a_0	9.9132747650×10^0	0.7905374169×10^0
a_1	$-5.2367539406 \times 10^0$	$-4.4604940414 \times 10^0$
a_2	1.2129990387×10^2	5.3346576691×10^1
a_3	$-2.1271813965 \times 10^3$	$-7.3640325928 \times 10^2$
a_4	2.2541205078×10^4	6.9652080078×10^3
a_5	$-1.4416690625 \times 10^5$	$-4.2423710938 \times 10^4$
a_6	5.4555181250×10^5	1.5623592187×10^5
a_7	$-1.1230468750 \times 10^6$	$-3.1305646875 \times 10^5$
a_8	9.7031368750×10^5	2.5589892187×10^5
β_1	2.649242	1.693474
β_2	1.333239	1.047213

Table 2. Spectroscopic constants of OH^+ and H_2 diatoms, with the unit of R_e in a.u. (atomic unit), D_e in unit kcal/mol, and ω_e, $\omega_e x_e$, α_e, and β_e in unit cm^{-1}.

	R_e	D_e	ω_e	$\omega_e x_e$	α_e	β_e
			$OH^+(X\,^3\Sigma^-)$			
This work	1.9430	5.2972	3058.71	54.745	0.446	16.819
Theor.[4]	1.9428	5.1268	3126.60	–	–	–
Theor.[5]	1.9445	5.2818	3127	–	–	–
Theor.[41]	1.9460	5.2020	3113.37	78.515	0.750	16.794
Exp.[42]	1.9443	5.301	3113.37[a]	–	–	–
			$H_2(X\,^1\Sigma_g^+)$			
This work	1.4025	4.7479	4395.22	126.119	2.221	60.735
Theor.[4]	1.4010	4.7321	4351.24	–	–	–
Theor.[43]	1.4010	4.7477	4403.60	126.602	2.232	60.864
Theor.[44]	1.4013	4.7105	4389.66	121.560	3.162	60.826
Exp.[42]	1.4014	4.476	4395.20	117.99	2.993	60.809
Exp.[45]	1.4011	4.4781[b]	4401.21	121.33	3.062	60.853

[a] Ref. [46], [b] Ref. [47].

By subtracting the two-body energies from the total *ab initio* energies, for a given triatomic geometry, one can obtain the three-body energies, which are then fitted to the three-body term $V^{(3)}$ written as the M-th order polynomial[36,37,39,40]

$$V^{(3)}(R_1,R_2,R_3) = \begin{cases} \sum_{i,j,k=0}^{M} C_{ijk} \rho_1^i \rho_2^j \rho_3^k, & (k = l), \\ \sum_{i,j,k=0}^{M} C_{ijk} \rho_1^i (\rho_2^j \rho_3^k + \rho_3^j \rho_2^k), & (k \neq l), \end{cases} \quad (11)$$

where $\rho_i = R_i e^{-\beta_i^{(3)} R_i}$ $(i = AB, BC, AC)$. C_{jkl} and $\beta_i^{(3)}$ are the linear and nonlinear parameters to be determined in the fitting procedure. The two expressions of Eq. (11) are used to satisfy the permutation symmetry of the two H atoms. The constraints $i+j+k \neq i \neq j \neq k$ and $i+j+k \leq M$ are used to warrant that the three-body term becomes zero at all dissociation limits and when at least one of the internuclear distances is zero. M equals 10 in the present work, which results in a complete set of parameters to be determined amounting to a

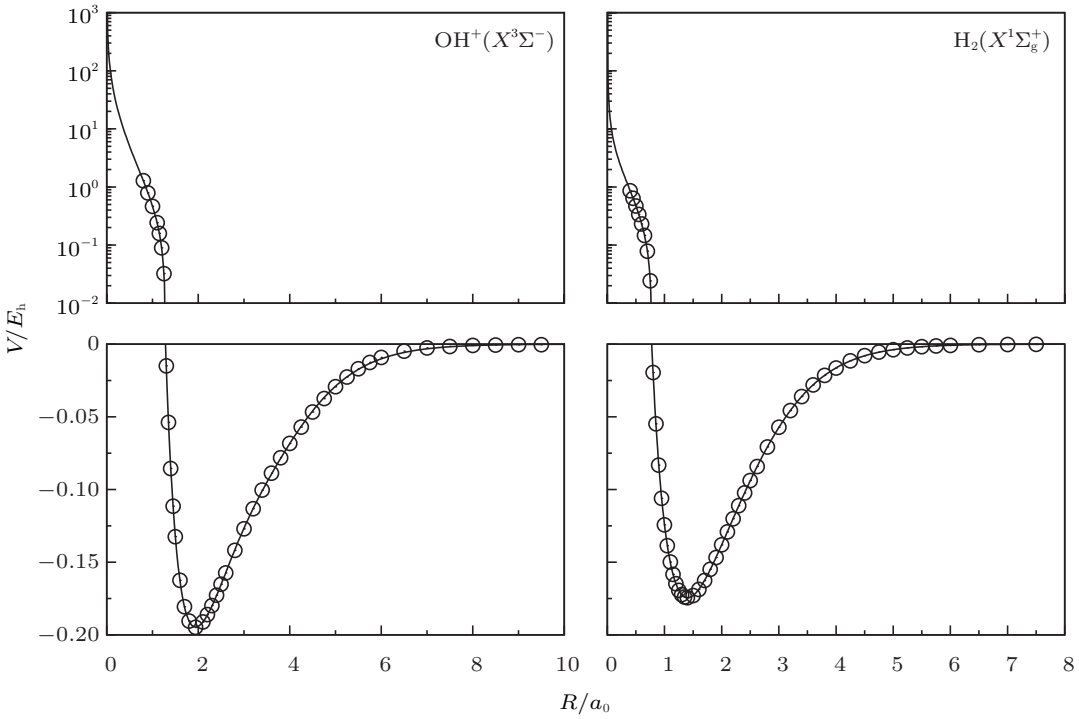


Fig. 1. Potential energy curves of $OH^+(X^3\Sigma^-)$ and $H_2(X^1\Sigma_g^+)$. The circles indicate the AVQZ/DMBE-SEC energies.

total number of 140 linear coefficients C_{ijk} and two nonlinear parameters (i.e., $\beta^{(3)}_{OH^+}$ and $\beta^{(3)}_{HH}$). A total of 2690 *ab initio* energies covering a range of energy up to 500 kcal/mol are employed in the fitting procedure, and the root-mean square derivation equals to 1.12 kcal/mol. The deviations between the fitted PES and the *ab initio* energies used in the fitting procedure are plotted in Fig. 2. It is observed that most of the *ab initio* energies locate in the range of derivation smaller than 1.0 kcal/mol. Explicitly, the number of *ab initio* energies with rmsd $<$ 1.0 kcal/mol is 1883, which occupies 70.03% of total *ab initio* energies, 431 *ab initio* energies with the derivation in the range of 1.0 kcal·mol^{-1} $\sim$ 1.5 kcal·mol^{-1}, and 187 *ab initio* energies locate in the range of derivation between 1.5 kcal·mol^{-1} and 2.0 kcal·mol^{-1}. Moreover, the number of *ab initio* energies with rmsd $>$ 2.0 kcal·mol^{-1} is 188, occupying only 6.99% of the total *ab initio* energies, which implies that the fitted PES is in good quality.

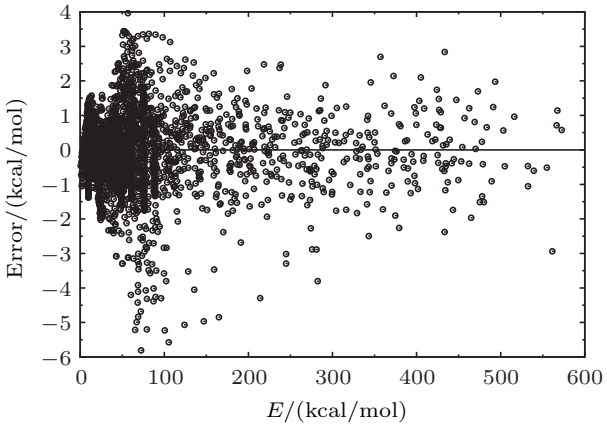


Fig. 2. Deviations between *ab initio* energies and the fitted PES of $H_2O^+(X^4A'')$.

4. Features of $H_2O^+(X^4A'')$ potential energy surface

Table 3 compares the attributes (geometries, energies, and vibrational frequencies) of the relevant stationary points of the current PES with other theoretical results for $H_2O^+(X^4A'')$: $C_{\infty v}[OHH]^+$, $C_{2v}[OH_2]^+$, and $C_{\infty v}[HOH]^+$ minima, and $D_{\infty v}[HOH]^+$ transition state. Also showing in this table are the results obtained by optimizing at MRCI/AVQZ level of theory in the present work, and at CCSD(T)/cc-pVQZ level of theory by Martínez *et al.*[4] As is shown in Table 3, the $C_{\infty v}[OHH]^+$ minimum located at $R_1 = 2.2950a_0$ (R_{H2}), $R_2 = 2.1209a_0$, and $R_3 = 4.4159a_0$ (R_{OH^+}). Comparing with the result calculated from analytical PES of Martínez *et al.*,[4] the derivations are only $0.0573a_0$, $0.0336a_0$, and $0.0237a_0$, respectively. The well depth calculated from the present PES is $0.2080E_h$ relative to the $O^+(^4S) + H(^2S) + H(^2S)$ asymptote, which is $0.006E_h$ lower than the results of Martínez *et al.*, [4] since the present PES is obtained by fitting *ab initio* energies calculated with higher accuracy, namely MRCI/AVQZ. Comparing with the well depth of the other minima and transition state, the $C_{\infty v}[OHH]^+$ minimum has the lowest energy, which is attributed to the global minimum of $H_2O^+(X^4A'')$. Both the well depth and geometry are in good accordance with the results obtained in the present work through optimization at MRCI/AVQZ level of theory, with the well depth differing

Table 3. Properties of stationary points on the fitted $H_2O^+(X\,^4A'')$ PES [a].

Feature	R_1/a_0	R_2/a_0	R_3/a_0	E/E_h [a]	ω_{sym}	ω_{asym}	$\omega_{bending}$
				$C_{\infty v}[OHH]^+$ minimum			
This work[c]	2.2950	2.1209	4.4159	–0.2080	1746.27	863.03	562.55
MRCI/AVQZ[d]	2.3011	2.1326	4.4337	–0.2072	1747.92	796.11	719.09
Ab initio[e]	2.2396	2.1545	4.4391	–0.2029	1643.42	767.59	763.00
Analytical fit[f]	2.2377	2.1545	4.3922	–0.2029	1644.09	785.04	765.04
				$C_{2v}[OH_2]^+$ minimum			
This work[c]	1.4945	3.4241	3.4241	–0.1954	823.19	326.29	3652.18
MRCI/AVQZ[d]	1.4929	3.5563	3.5563	–0.1970	743.66	556.33	3665.22
Ab initio[e]	1.5101	3.2585	3.2585	–0.1929	744.11	108.33	3582.54
Analytical fit[f]	1.5101	3.5890	3.5890	–0.1929	736.02	192.66	3401.79
				$C_{\infty v}[HOH]^+$ minimum			
This work[c]	8.3805	6.4362	1.9443	–0.1944	90.69	3050.63	99.00
MRCI/AVQZ[d]	7.6157	5.6733	1.9424	–0.1933	199.61	3127.53	65.39
Ab initio[e]	7.6108	5.6679	1.9429	–0.2029	171.71	3131.67	44.00
Analytical fit[f]	8.4102	6.4579	1.9523	–0.1913	286.26	3074.26	97.70
				$D_{\infty v}[HOH]^+$ transition state			
This work[c]	5.4107	2.7053	2.7053	–0.1230	1519.61	2507.02*i*	456.82
MRCI/AVQZ[d]	5.3144	2.6572	2.6572	–0.1265	1438.66	3618.64*i*	841.35
Ab initio[e]	5.2994	2.6497	2.6497	–0.1215	1416.07	2759.75*i*	860.59
Analytical fit[f]	5.4922	2.7461	2.7461	–0.1224	1204.39	1759.44*i*	675.72

[a] Harmonic frequencies in unit cm^{-1}. [b] Energy relative to the three-atom limit $O^+(^4S)+H(^2S)+H(^2S)$. [c] This work, fitted by the current analytical PES. [d] This work, obtained through optimization at the MRCI/AVQZ level of theory. [e] *Ab initio* results calculated at CCSD(T)/cc-pVQZ level of theory.[4] [f] From the analytical PES of Martínez *et al.*[4]

by $0.0008E_h$ and the maximal difference $0.0789a_0$ of geometries occurs for OH bond length. The harmonic vibrational frequencies for the $C_{\infty v}[OHH]^+$ minimum obtained by the present PES are 1746.27 cm^{-1}, 863.03 cm^{-1}, and 562.55 cm^{-1}, which are also in good agreement with the results through optimization searches at the MRCI(Q)/AVQZ level (1747.92 cm^{-1}, 796.11 cm^{-1}, and 719.09 cm^{-1}), and the results of analytical PES obtained by Martínez *et al.*[4] (1644.09 cm^{-1}, 785.04 cm^{-1}, and 765.04 cm^{-1}).

The major topographical features of the $H_2O^+(X\,^4A'')$ PES reported in the present work are displayed in Figs. 3–7. The salient features from these contour plots are some of the most relevant stationary points for the title system. Clearly, a smooth and correct behavior can be observed over the whole configuration space. Figure 3 shows a contour plot for the C_{2v} insertion of O^+ into H_2 diatom from large atom–diatom separations along T-shaped geometries. In this process, when the O^+ inserts into H_2 diatom, the $\angle HOH$ opens progressively, while the separation between O^+ and the center of H–H shortens, and the bond length of H–H increases. It can be seen from this figure that there exists a local minimum ($C_{2v}[OH_2]^+$) locating at $x \approx 1.5a_0$ and $y \approx 3.3a_0$ ($R_1 = 1.4945a_0$, $R_2 = R_3 = 3.4241a_0$), with the well depth lying at $-0.1954E_h$ which is 8.5341 kcal·mol^{-1} above the $C_{\infty v}[OHH]^+$ minimum, and the harmonic vibrational frequencies being 1577, 562, and 1886 cm^{-1}, respectively. The geometry, well depth, and harmonic vibrational frequencies compare well with the results obtained by Martínez *et al.*[4] Another notable feature shown in this figure is the $D_{\infty v}[HOH]^+$ transition state lies at $R_1 = 5.1406a_0$ and $R_2 = R_3 = 2.7053a_0$, with the barrier height of $-0.1230E_h$ which is 53.338 kcal·mol^{-1} above $C_{\infty v}[OHH]^+$ minimum and 44.804 kcal·mol^{-1} above the $C_{2v}[OH_2]^+$ minimum. Comparing with the results of Martínez *et al.*:[4] the bond length differences are calculated to be $0.0816a_0$ and $0.0408a_0$, and the well depth predicted by the current PES is 3.7651 kcal·mol^{-1} deeper. The harmonic vibrational frequencies are of $D_{\infty v}[HOH]^+$ transition state are calculated to be 1519.61 cm^{-1}, 2507.02i cm^{-1}, and 456.82 cm^{-1}, with the MRCI/AVQZ results being 1438.66 cm^{-1}, 3618.64i cm^{-1}, and 841.35 cm^{-1}. In turn, the results obtained from the analytical PES by Martínez *et al.*[4] are 1204.39 cm^{-1}, 1759.44i cm^{-1}, and 675.72 cm^{-1}, with the CCSD(T)/cc-pvQZ results being 1416.07 cm^{-1}, 2759.75i cm^{-1}, and 860.59 cm^{-1}. As seen from Table 3, the results from the current PES show overall good agreement with the results of Martínez *et al.*[4]

Figure 4 shows a contour plot for both OH^+ stretching in H–O–H^+ linear configuration. The notable features shown in Fig. 4 are the two equivalent asymmetric hydrogen-bonded minima, which are connected by a barrier lying at $R_2 = R_3 = 2.7053a_0$. Figure 5 shows the contour plot for bond

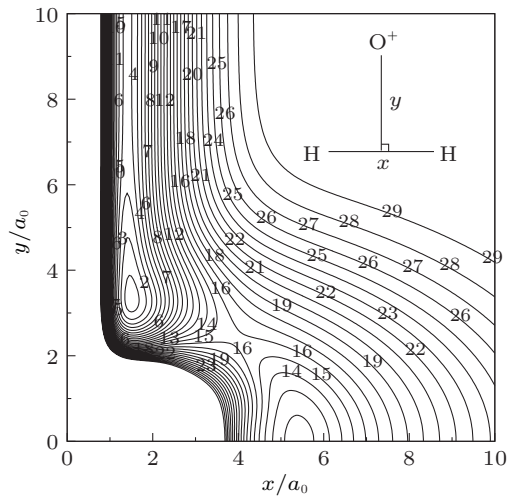


Fig. 3. Contour plot for C_{2v} insertion of O^+ into H_2 diatom. Contours equally spaced by $0.0065\,E_h$, starting at $-0.192\,E_h$.

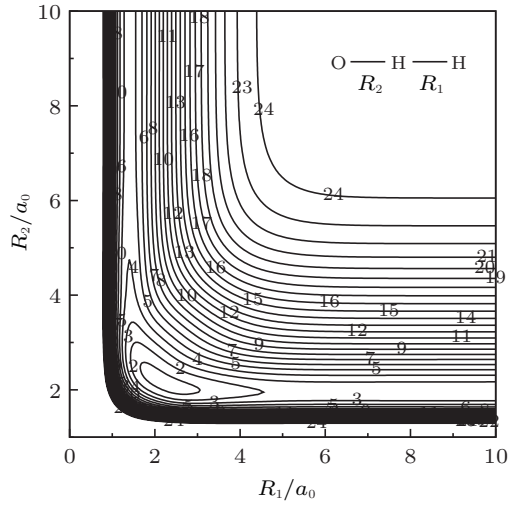


Fig. 5. Contour plot for bond stretching in $[O–H–H]^+$ collinear configuration. Contours equally spaced by $0.0085\,E_h$, starting at $-0.205\,E_h$.

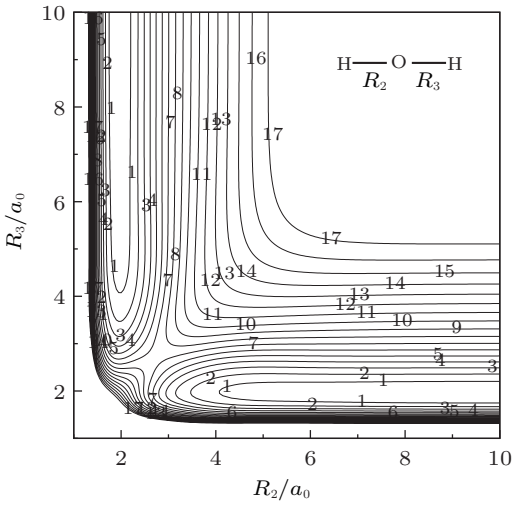


Fig. 4. Contour plot for bond stretching in $[H–O–H]^+$ linear configuration. Contours equally spaced by $0.004\,E_h$, starting at $-0.1158\,E_h$.

stretching of OH^+ and HH in $O–H–H^+$ collinear configuration. A minimum can be seen to locate at $R_1 = 2.2950a_0$, and $R_2 = 2.1209a_0$, which is attributed to be the $C_{\infty v}[OHH]^+$ minimum. Also visible in this figure is O^+ can approach HH diatom via a barrierless process from large atom–diatom separations along the $O–H–H^+$ collinear configurations, thus agreeing with findings of Martínez *et al.*[4]

Figure 6 shows a contour plot for an H atom moving around an OH^+ diatom with the bond length of OH^+ fixed at equilibrium geometry $R_{OH^+} = 1.943a_0$, which lies along the X axis with the center of the bond fixed at the origin. One of the salient features is the $C_{\infty v}[OHH]^+$ minimum exists when H approaches OH^+ collinearly, which can also be seen in Fig. 5. In turn, figure 7 shows a contour plot for O^+ atom moving around a fixed HH diatom with the bond length fixed at equilibrium geometry $R_{HH} = 1.401\,a_0$, which lies along the X axis

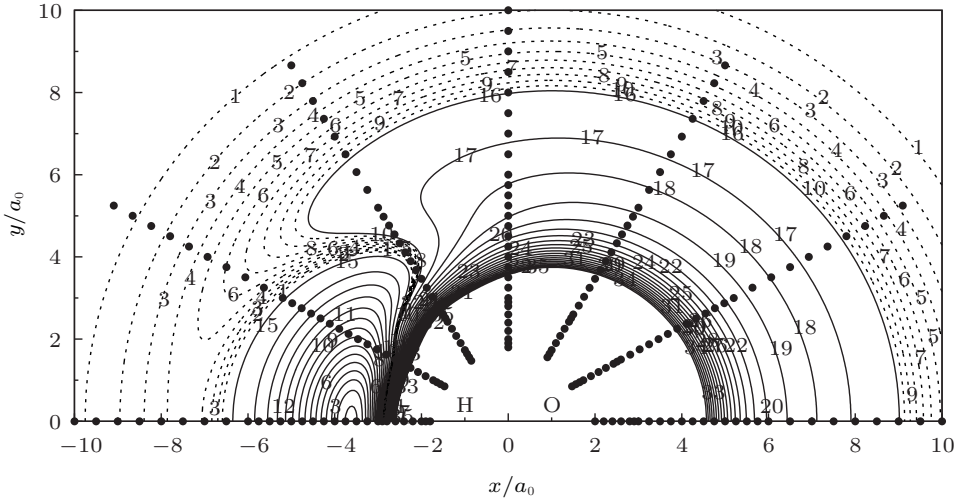


Fig. 6. Contour plot for H atom with the coordinate (x, y) moving around a fixed OH^+ diatom with the bond length fixed at $R_{OH^+} = 1.943\,a_0$, which lies along the X axis with the center of the bond fixed at the origin. Contours are equally spaced by $0.0008\,E_h$, starting at $-0.21\,E_h$. The dashed lines are contours equally spaced by $-0.00006\,E_h$, starting at $-0.1946\,E_h$. Also shown are the calculated *ab initio* points for the H atom moving around OH^+ diatom.

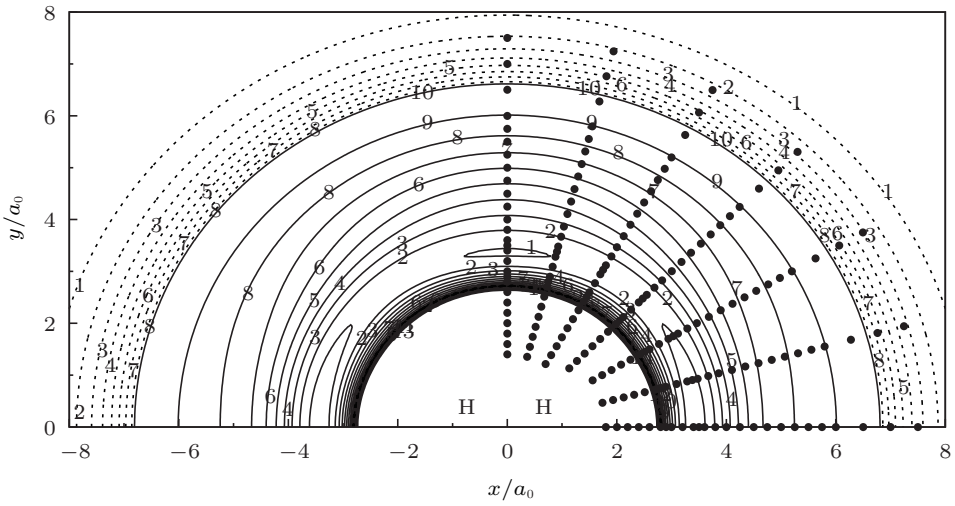


Fig. 7. Contour plot for O^+ with the coordinate (x, y) moving around a fixed H_2 diatom in equilibrium geometry $R_{H_2} = 1.401\,a_0$, which lies along the X axis with the center of the bond fixed at the origin. Contours are equally spaced by $0.002\,E_h$, starting at $-0.196\,E_h$. The dashed area is contours equally spaced by $-0.0002\,E_h$, starting at $-0.1745\,E_h$. Also shown are the calculated *ab initio* points for the O^+ atom moving around H_2 diatom.

with the center of the bond fixed at the origin. As can be seen in this figure, there exist a C_{2v} and two equivalent $C_{\infty v}$ minima in the process of O^+ moving around the fixed HH diatom. Also shown in Figs. 6 and 7 are the *ab initio* energies utilized in the fitting procedure, which cover both the short and long regions, warranting the reliable behavior of the current PES. These two contour plots clearly reveal a smooth behavior both at short and at long-range regions.

5. Concluding remarks

A wealth of accurate MRCI/AVQZ energies have been calculated in the present work to map the PES of $H_2O^+(X\,^4A'')$. The resulting raw energies have been corrected subsequently using the DMBE-SEC method and then utilized in the fitting procedure to obtain the globally accurate PES, which is expected to be realistic over the entire configuration space. The various topographical features of the current PES have been examined in detail and compared with the previous theoretical results. The properties of several minima and transition states, including the geometries, energies, and vibrational frequencies, have been characterized on the current $H_2O^+(X\,^4A'')$ PES, which agree nicely with the topographical predictions of other theoretical work. Based on such features, it is concluded that the PES here reported is globally valid while accurately fitting the *ab initio* points utilized for its calibration. Thus, the present $H_2O^+(X\,^4A'')$ PES should be valuable for studying the kinetics and dynamics of reactions involving ground-state H_2O^+, such as $O^+(^4S) + H_2(X\,^1\Sigma_g^+)$, which is currently in progress.

References

[1] Duley W W and Williams D A 1984 *Interstellar Chemistry* (New York: Academic Press)

[2] Ng C Y 2002 *J. Phys. Chem. A* **106** 5953

[3] González M, Gilibert M, Aguilar A and Sayós R 1993 *J. Chem. Phys.* **98** 2927

[4] Martínez R, Millán J and González M 2004 *J. Chem. Phys.* **120** 4705

[5] Paniagua M, Martínez R, Gamallo P and González M 2014 *Phys. Chem. Chem. Phys.* **16** 23594

[6] Fehsenfeld F C, Schmeltekopf A L and Ferguson E E 1967 *J. Chem. Phys.* **46** 2802

[7] Smith D, Adams N G and Miller T M 1978 *J. Chem. Phys.* **69** 308

[8] Viggiano A A, Van Doren J M, Morris R A, Williamson J S, Mundis P L, Paulson J F and Dateo C E 1991 *J. Chem. Phys.* **95** 8120

[9] Li X, Huang Y L, Flesch G D and Ng C Y 1997 *J. Chem. Phys.* **106** 564

[10] Sunderlin L and Armentrout P 1990 *Chem. Phys. Lett.* **167** 188

[11] Gillen K T, Mahan B H and Winn J S 1973 *J. Chem. Phys.* **58** 5373

[12] Gillen K T, Mahan B H and Winn J S 1973 *J. Chem. Phys.* **59** 6380

[13] González M, Aguilar A and Gilibert M 1989 *Chem. Phys.* **131** 335

[14] González M, Aguilar A and Gilibert M 1989 *Chem. Phys.* **131** 347

[15] Whitton W, Mahling S and Kuntz P 1992 *Chem. Phys.* **162** 379

[16] Martínez R, Sierra J D and González M 2005 *J. Chem. Phys.* **123** 174312

[17] Martínez R, Sierra J D, Gray S K and González M 2006 *J. Chem. Phys.* **125** 164305

[18] Martínez R, Lucas J M, Giménez X, Aguilar A and González M 2006 *J. Chem. Phys.* **124** 144301

[19] Kłos J, Bulut N and Akpinar S 2012 *Chem. Phys. Lett.* **532** 22

[20] Xu W, Li W, Lv S, Zhai H, Duan Z and Zhang P 2012 *J. Phys. Chem. A* **116** 10882

[21] Xu W, Li W and Zhang P 2013 *Comput. Theor. Chem.* **1012** 1

[22] Werner H J and Knowles P J 1988 *J. Chem. Phys.* **89** 5803

[23] Kendall R A, Dunning T H Jr and Harrison R J 1992 *J. Chem. Phys.* **96** 6796

[24] Dunning T H Jr 1989 *J. Chem. Phys.* **90** 1007

[25] Knowles P J and Werner H J 1985 *Chem. Phys. Lett.* **115** 259

[26] Varandas A J C 1989 *J. Chem. Phys.* **90** 4379

[27] Zhang L L, Gao S B, Meng Q T and Song Y Z 2015 *Chin. Phys. B* **24** 013101

[28] Varandas A J C and Rodrigues S P J 2006 *J. Phys. Chem. A* **110** 485

[29] Song Y Z, Caridade P J S B and Varandas A J C 2009 *J. Phys. Chem. A* **113** 9213

[30] Song Y Z and Varandas A J C 2011 *J. Phys. Chem. A* **115** 5274

[31] Molpro version 2012.1 a package of *ab initio* programs, Werner H J, Knowles P J, Knizia G, Manby F R, Schütz M and others 2012 see http://www.molpro.net

[32] Varandas A J C and Poveda L A 2006 *Theor. Chem. Acc.* **116** 404

[33] Li Y Q, Song Y Z, Song P, Li Y Z, Ding Y, Sun M T and Ma F C 2012 *J. Chem. Phys.* **136** 194705
[34] Song Y Z, Li Y Q, Gao S B and Meng Q T 2014 *Eur. Phys. J. D* **68** 1
[35] Murrell J N and Carter S 1984 *J. Phys. Chem.* **88** 4887
[36] Aguado A and Paniagua M 1992 *J. Chem. Phys.* **96** 1265
[37] Aguado A, Tablero C and Paniagua M 1998 *Comput. Phys. Comm.* **108** 259
[38] Liao J W and Yang C L 2014 *Chin. Phys. B* **23** 073401
[39] Liang J J, Yang C L, Wang L Z and Zhang Q G 2012 *J. Chem. Phys.* **136** 094307
[40] Yang C L, Wang L Z, Wang M S and Ma X G 2013 *J. Phys. Chem. A* **117** 3
[41] Riahi R, Teulet P, Cressault Y, Gleizes A and Ben Lakhdar Z 2008 *Eur. Phys. J. D* **49** 185
[42] Huber K P and Herzberg G 1979 *Molecular Spectra and Molecular Structure IV: Constants of Diatomic Molecules* (New York: Van Nostrand Reinhold)
[43] Varandas A J C 1996 *J. Chem. Phys.* **105** 3524
[44] Yang C L, Huang Y J, Zhang X and Han K L 2003 *J. Mol. Struct.: THEOCHEM* **625** 289
[45] Huber K P G H 2001 *NIST Chemistry WebBook* 69 http://webbook.nist.gov/chemistry
[46] Hirst D M and Guest M F 1983 *Mol. Phys.* **49** 1461
[47] Balakrishnan A, Smith V and Stoicheff B P 1992 *Phys. Rev. Lett.* **68** 2149